Escherichia coli versus *Pseudomonas aeruginosa* Deacetylase LpxC Inhibitors Selectivity: Surface and Cavity-Depth-Based Analysis

Rameshwar U. Kadam,[†] Amol V. Shivange,[‡] and Nilanjan Roy*[,†,‡]

Centre of Pharmacoinformatics and Department of Biotechnology, National Institute of Pharmaceutical Education and Research, Sector 67, S. A. S. Nagar, Punjab 160062, India

Received November 1, 2006

Although *Escherichia coli* and *Pseudomonas aeruginosa* LpxC share sequence and functional similarity, *E. coli* LpxC inhibitiors are ineffective against *P. aeruginosa* LpxC. It was earlier speculated that inactivity of the inhibitors is due to intrinsic resistance possibly mediated by efflux pumps. However, a recent study has documented that the inactivity is due to failure of inhibitor(s) to inhibit the enzyme rather then intrinsic resistance. In this study, we carried out a surface and cavity-depth-based analysis on homology models of *E. coli* and *P. aeruginosa* LpxC to get some new insights into the ligand-binding features of these enzymes. The surface analysis of the *P. aeruginosa* LpxC model suggested that the LpxC catalytic domain (where inhibitors are supposed to bind) has several minor but potentially important structural differences as compared to *E. coli* LpxC. Molecular docking studies which could distinguish between the reported receptor affinities of the inhibitors additionally helped in the identification of key binding-site residues and interactions. These differences can be exploited for designing broad-spectrum LpxC inhibitors against this target.

INTRODUCTION

The current medical cure of Gram-negative bacterium infections involves a combination therapy of antibiotics, such as β-lactams (ticarcillin), carbapenems (imipenem-cilastatin and meropenem), aminoglycosides (tobramycin), and so forth. However multidrug-resistant strains of the pathogen have evolved which substantiate the need of identification and development of novel antibacterial targets (http://www.emedicine.com/med/topic1943.htm). A detailed analysis of the outer leaflet of the outer membrane of a Gram-negative bacterium has been performed by Whittington et al. to identify such novel antibacterial targets. The outer leaflet is composed of lipopolysaccharide (LPS), which serves as a permeability barrier that protects the bacterium against antibiotics.[1−6] Each LPS molecule contains three main components: an immunodominant and highly variable repeating oligosaccharide known as the O-antigen, a core polysaccharide and lipid A (the hydrophobic anchor of LPS). Lipid A is a phosphorylated, β(1,6)-linked glucosamine disaccharide hexaacylated with N-linked and O-linked fatty acids, which is essential for LPS assembly in the outer membrane and consequently the viability of the Gram-negative bacterium.[4−6] Thus, accordingly, Lipid A and its biosynthesis have attracted attention as a therapeutic target for the treatment of Gram-negative bacterial infections.[5−10] The first committed step in lipid A biosynthesis is catalyzed by a metal-dependent deacetylase, UDP-{3-*O*- [(*R*)-3-hydroxymyristoyl]}-*N*-acetylglucosamine deacetylase, also known as LpxC, which hydrolyzes *N*-acetylglucosamine to form acetate and glucosamine (Figure 1a).[11−14]

Thus, recently, several laboratories have focused on this metalloenzyme which has also been demonstrated to be essential for the growth of *Escherichia coli*.[15−17] Though, the essentiality of LpxC activity for *Pseudomonas aeruginosa* has not been proven experimentally however, the lack of a mutated *LpxC* gene in a saturating transposon mutagenesis study indicated that this gene might be essential.[18] The LpxC protein of *P. aeruginosa* is encoded by a homologous gene (Figure 2b) and catalyzed the same step[19] in a saturating transposon mutagenesis study as that seen in *E. coli*. These data on sequence similarity and functional identity suggest that it could be possible to discover LpxC inhibitors active against both *E. coli* and *P. aeruginosa*. However, none of the early LpxC inhibitors, which showed antibacterial activity against *E. coli* and certain other organisms, were able to inhibit the growth of *P. aeruginosa*.[20−23] It was assumed that the reason for this failure was the intrinsic resistance of *P. aeruginosa* to antibiotics. However, a study by Erwin et al.,[22] who placed the *lpxC* gene of *P. aeruginosa* under the tight control of an arabinose-inducible promoter, demonstrated that the *P. aeruginosa* LpxC gene itself is the primary factor in resistance to inhibitors; membrane impermeability or inhibitor efflux plays a relatively minor role. Although this study indicated the possibility of structural differences of *E. coli* and *P. aeruginosa* LpxC, it was unable to give a detailed mechanism for the selectivity of the series of synthetic LpxC inhibitors toward *E. coli*.

Thus, to study the potentially important structural differences in active sites of both proteins responsible for making the inhibitors selective for *E. coli* as compared to *P. aeruginosa* LpxC, homology models of the LpxC of both organisms were developed and validated on the basis of a 3D profile and PROCHECK. Subsequently, a molecular electrostatic potential (MEP)-based surface and cavity-depth analysis was performed. Finally, a cross-docking analysis

* Corresponding author tel.: +91 172 2214 682-87 ext 2067; fax: +91 172 2214 692, e-mail :nilanjanroy@niper.ac.in.
[†] Centre of Pharmacoinformatics.
[‡] Department of Biotechnology.

10.1021/ci6004806 CCC: $37.00
Published on Web 04/19/2007

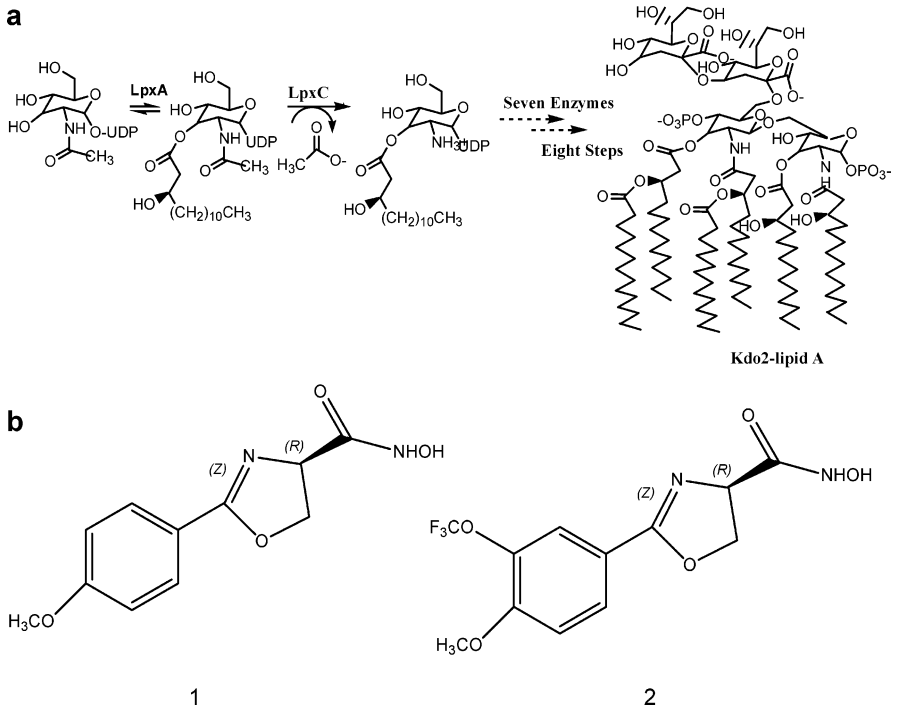

Figure 1. Deacetylation of UDP-(3-O-acyl)-N-acetylglucosamine and LpxC inhibitors. LpxC catalyzes the second step in the biosynthesis of lipid A. Because the first step is reversible, the LpxC reaction is the first committed step in the conversion of UDP-N-acetylglucosamine to lipid A (a). Structure of the LpxC inhibitor **1** and **2** (b).

of reported inhibitors (Figure 1b)[20,23] was performed to reveal selective binding modes. These studies identified differences between the two active sites and have implications for designing effective strategies to identify LpxC inhibitors that can be developed as novel broad-spectrum antibacterial drugs.

METHODOLOGY

All computations and molecular modeling of *E. coli* and *P. aeruginosa* LpxC were carried out on a Silicon Graphics Fuel workstation with the IRIX 7.1 operating system using the MOE-06 (Molecular Operating Environment)[24] and SYBYL7.1[25] molecular modeling packages. A homology modeling module of MOE was used for model development, and a molecular docking study was performed using the FlexX module in SYBYL7.1.

Homology Modeling. The amino acid sequences of *E. coli* LpxC and *P. aeruginosa* LpxC were obtained from the Swiss-Prot protein database (*E. coli*, SWISS-PROT accession no. P0A727; *P. aeruginosa*, SWISS-PROT accession no. P47205). NCBI-BLAST (http://www.ncbi.nlm. nih.gov/BLAST/)[26] was used to identify the template structures from the Protein Data Bank (PDB)[27] for modeling the two proteins (Table 1).

1. Sequence Alignment. For the *E. coli* LpxC sequence alignment, sequences were obtained from the PDB structure files of the selected templates including *Aquifex aeolicus* deacetylase LpxC (1P42)[28]and Aalpxc TU-514 complex (1XXE).[29] For the *P. aeruginosa* LpxC sequence alignment, sequences were extracted from the PDB structure files of the selected templates including *Aquifex aeolicus* deacetylase LpxC (1P42), Aalpxc TU-514 complex (1XXE), and TNSA, a catalytic component of the TN7 transposition system (1F1Z).[30] As mentioned above, template sequences were aligned with the respective query sequence using pairwise sequence alignment (local and global) in EMBOSS-GUI (http://bioinfo.hku.hk/EMBOSS/).

The structurally conserved regions (SCRs) in template proteins were then identified. *E. coli* LpxC and *P. aeruginosa* LpxC sequences were subsequently aligned to the SCRs using the alignment module and finally fine-tuned manually (Figure 2a,b).

2. Loop and End Region Modeling. Three variable regions L44 to P47, I186 to S188, and N176 to S178 of *E. coli* LpxC and two variable regions L44 to V47 and T179 to V182 of *P. aeruginosa* LpxC were found to have very little homology to the template proteins. These were thus modeled with the ProDat loop modeling algorithm.

3. Side-Chain Rotamer Search. The possible ranges of stable conformations for certain residues in side chains and the interacting residues were explored with a rotamer search module in MOE. This method was used to monitor any possible steric clashes, which were then relieved appropriately.

4. Model Building. A homology modeling module of MOE was used for the model building of both proteins. A total of 10 independent models were constructed by the Boltzmann-weighted randomized modeling procedure. Each of these intermediate models was subjected to a sufficient degree of minimization to relieve any serious steric clashes using coarse model refinement. The model with the best packing quality was chosen for further development.

5. Addition of Zn^{2+} and Water Molecules. Zn^{2+} and water molecules were added to the models using MOE and optimized using an MMFF94 force field and PM3, a gradient 0.01 kcal/mol Å Hamiltonian, in MOE. The optimized geometric parameters and the metal ions were used for optimization of the three-dimensional structure of both proteins. Models were further refined by energy minimization to remove any steric clashes among the side chains and/or

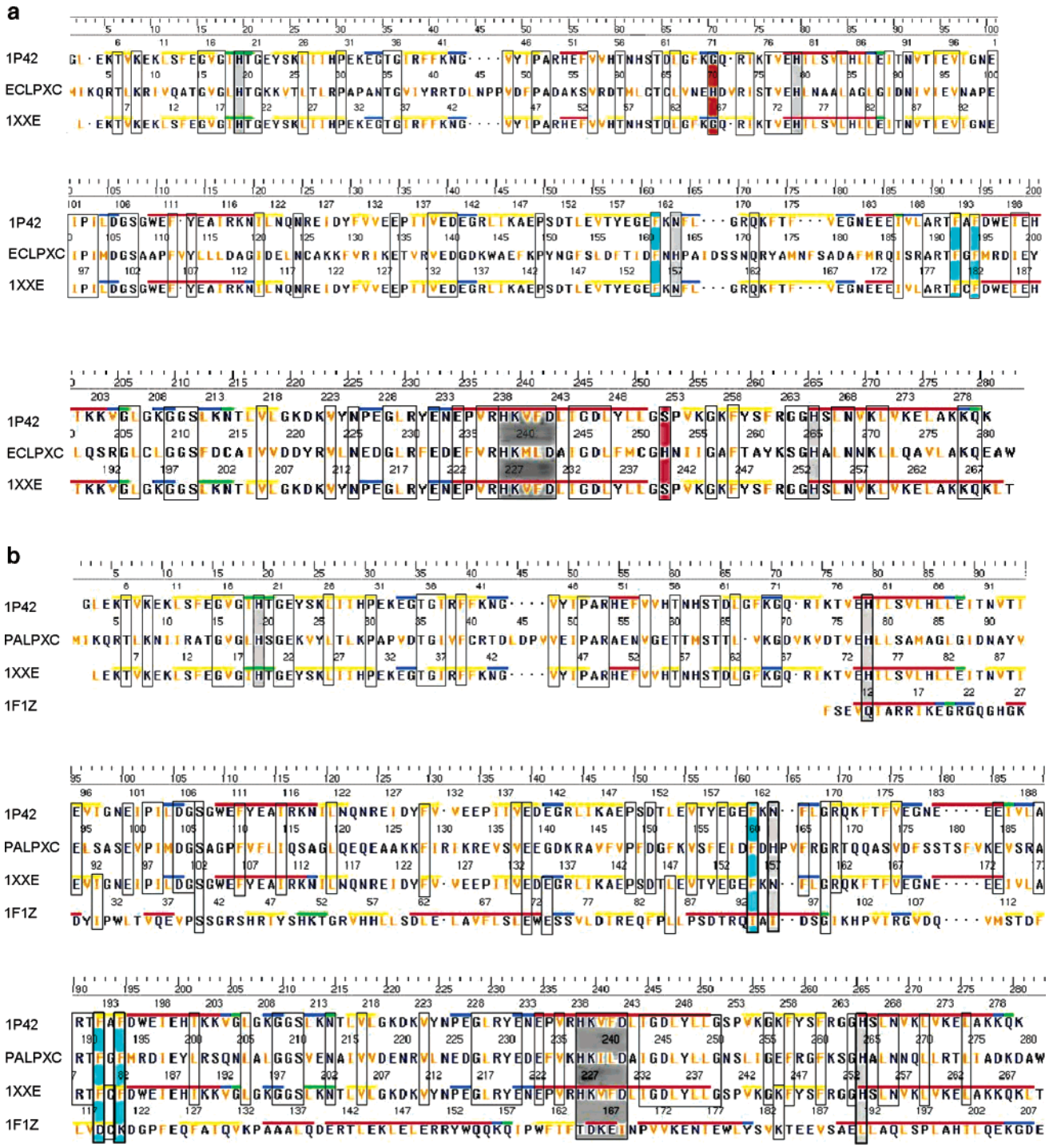

Figure 2. Multiple sequence alignment of the LpxC. *E. coli* LpxC (ECLPXC), *Aquifex aeolicus* LpxC deacetylase (1P42), and AalpxcTU-514 complex (1XXE) (a). Multiple sequence alignment of the *P. aeruginosa* LpxC (PALPXC) (b): *Aquifex aeolicus* LpxC deacetylase (1P42), AalpxcTU-514 complex (1XXE), and TNSA, a catalytic component of the TN7 transposition system (1F1Z) based on the sequence homology. The identical residues are highlighted in hollow boxes. The novel zinc binding motif characteristic of all known LpxC enzymes, HKXXD, is shown in a dark gray box. Four other conserved histidines are shown in light gray boxes, and two *E. coli* histidines that are absent from *P. aeruginosa* are shown in red-orange boxes. The conserved phenylalanines providing a hydrophobic patch are shown in cyan boxes. Solid red, blue, and gray underlines indicate the secondary structural elements.

with backbone atoms. For this, the models were first subjected to a highly tethered series of conjugate gradient minimization steps. The three available minimization options including coarse, medium, and fine use the truncated Newton optimization algorithm, with root-mean-square (RMS) gradient tests of 10, 1, and 0.1 Å, respectively. The medium option was selected for the reported modeling.

6. Validation of E. coli LpxC and P. aeruginosa LpxC Model. The final models were inspected for accuracy and validity using 3D-profile programs (http://nihserver.mbi.ucla.edu/Verify_3D/)[31] which calculate a 3D-to-1D compatibility score, and the graphical representation portrays the properly folded and misfolded regions in the protein structure by performing an Eisenberg analysis of the model. The

Table 1. Selected Templates for Homology Modeling of the *E. coli* LpxC and *P. aeruginosa* LpxC

name	source	local identity (%)	PDB ID	resolution (Å)
P. aeruginosa LpxC	*Aquifex aeolicus* deacetylase LpxC	37.1%	1P42	2.00
	AalpxcTU-514 complex	37.1%	1XXE	NA
	TNSA, a catalytic component of the TN7 transposition system	23.1%	1F1Z	2.40
E. coli LpxC	*Aquifex aeolicus* deacetylase LpxC	32.9%	1P42	2.00
	AalpxcTU-514 complex	32.9%	1XXE	NA

stereochemistry of both models was further gauged using a Ramachandran plot within the PROCHECK server of the Biotech Validation Suite for Protein Structures (http://biotech.ebi.ac.uk:8400/)[32] and a protein report tool implemented in MOE.

Molecular Electrostatic Potential (MEP) and Cavity-Depth Analysis (CD). The electrostatic interactions are a crucial player in the nonbonded interaction energy between molecules. The electrostatic potential on a molecular surface can be used to visually compare different molecules and as a useful tool for guiding docking studies. The molecular electrostatic potential on a protein surface can be used to find sites that act attractively on ligands by matching opposite electrostatics. MEP is calculated by the following equation:

$$\mathrm{EP}(i) = \sum_{j=1}^{N} \frac{qi}{rij}$$

where EP(*i*) is the electrostatic potential at the surface point *i* due to atom *j* having the partial charge *qi* and separated by distance *rij*. The EP on the surface is generally colored according to the sign and magnitude of the potential. The color ramp for EP ranges from red (most positive) to purple (most negative). For a better understanding of differences in active sites, MEP calculations and a cavity-depth analysis were performed.

All MEP and cavity-depth analysis calculations and visualizations were carried out using the MOLCAD program implemented in the SYBYL7.1 molecular modeling package. Gasteiger−Hückel charges were assigned to the atoms of both homology models (*E. coli* LpxC and *P. aeruginosa* LpxC), and surfaces were generated and visualized. Subsequently, a homology model of *E. coli* LpxC was superimposed onto the *P. aeruginosa* LpxC homology model, and corresponding residues within a 7 Å radius of the Zn^{2+} binding pocket were identified.

Docking Study. Known potent inhibitors of the *E. coli* and *P. aeruginosa* LpxC's were docked into the validated homology models. The molecule **1B1** has been reported as an inhibitor of *E. coli* LpxC by research at Merck,[20] and **1B2** has been reported as an inhibitor of *P. aeruginosa* LpxC by Kline et al.[23] For the present study, these molecules were built using SYBYL7.1 while maintaining the R configuration at the 4 position in the ring (a chiral center [(−C(═O)−NH(OH)]). Since the crystal structures of these LpxC inhibitors have not been determined, the basic skeleton and conformation for each molecule (i.e., **1B1** and **1B2**) were modeled using the *systematic conformation* search procedure in SYBYL7.1, and a lowest minima conformation was selected and minimized using the PM3 Hamiltonian using MOPAC interfaced with SYBYL7.1. In order to generate accurate charge information, a single-point energy calculation was also performed using the AM1 Hamiltonian[33] on the PM3-optimized geometry. Mulliken charges were assigned to both the molecules.[34] Docking experiments were carried out using the FlexX module in SYBYL7.1, which utilizes the incremental construction algorithm. The active site for docking was defined using the siteID module in SYBYL7.1. siteID identified the major pockets in the protein structures which could be probable binding sites. From these, one site for each protein was selected on the basis of the literature reports on the residues occurring in the active site and hydrophobic nature of the site.[35−37]

RESULTS AND DISCUSSION

As a first step toward the building of the homology model of *E. coli* and *P. aeruginosa* LpxC, a template search was carried out using NCBI-BLAST (http://www.ncbi.nlm.nih.gov/BLAST/). The results revealed the availability of two crystal structures 1P42 and 1XXE (with the resolutions 2.00 Å and NA, respectively) as templates for the *E. coli* LpxC modeling and three crystal structures 1P42, 1XXE, and 1F1Z (with the resolutions 2.00 Å, NA, and 2.40 Å, respectively) as templates for *P. aeruginosa* LpxC (Table 1).

In the case of the *E. coli* LpxC modeling sequence of the best hit, *Aquifex aeolicus* deacetylase LpxC (1P42) was aligned globally with the *E. coli* LpxC sequence using Needleman−Wunch dynamic programming to identify the overall similarity between the protein sequences (needle program in EMBOSS).[38] The identity and similarity between the target and template were 29.8% and 47.5%, respectively. To find out the local identity between the two sequences, local pairwise alignment was carried out using the dynamic programming technique (water program in EMBOSS package), which deciphered 32.9% identity and 52.3% similarity.

Similarly, for *P. aeruginosa* LpxC modeling, the sequence was aligned against the best hit, *A. aeolicus* deacetylase LpxC (1P42), whereby global alignment showed 33.2% identity and 52.6% similarity, and local alignment presented 37.1% identity and 58.5% similarity. For both proteins, these Web-based interpretations revealed a better alignment in the N-terminal regions containing the substrate-binding site of the enzyme. Further steps for model building were performed in MOE, as the automated modeling of MOE did not provide an option to use the desired templates for modeling; the templates were manually placed into MOE for the multiple alignments (Figure 2a,b).

The SCRs and structurally variable regions (SVRs) were defined, after which the models were built using *A. aeolicus* deacetylase LpxC as the primary template and selected residues from other templates of *E. coli* and *P. aeruginosa* LpxC. A total of 10 intermediate preliminary models were built for both cases. The best of the 10 models was chosen on the basis of good packing quality, determined by histogram-based application of a statistical packing quality

function. Similar to the energy function used in building candidate models, the packing quality function uses statistics gathered with a flexible atom-typing scheme extended to nonprotein atoms. Permutation selection of different loop candidates and side-chain rotamers and subsequent minimization to relieve any steric clashes led to models to which Zn^{2+} and water molecules were added. The presence of a unique zinc binding motif in LpxC has been reported in the literature.[35−37] The catalytic zinc ion in LpxC is coordinated by an HKX (L,F)D + H binding motif and a water molecule, which is consistent with observations from the X-ray crystallographic structure and mutagenesis data.[28−30,35−37] The crystal structure of the zinc-inhibited LpxC shows that the inhibitory zinc ion is coordinated by Glu78, His265, and bridged water molecule.[36,37] For the reported homology models, coordinates of Zn^{2+} and the water molecule in the active site were mimicked from the crystal structure of the primary template (Supporting Information, file1, Figure 1a,b). The distances between the atom pairs have been given in the Supporting Information (file 1, Tables 1 and 2). To improve the quality of both the models, refinement by molecular mechanics was carried out, in which the models were subjected to a highly tethered series of conjugate gradient minimization steps. The minimization option using the truncated Newton optimization algorithm, with a RMS gradient of 1 Å, was employed. Further refinement of the models of *E. coli* and *P. aeruginosa* LpxC was done by energy minimization of the selected outlier residues. These outlier residues were determined by the use of a protein report tool and Ramachandran plot of MOE; the chirality of the cis outliers was inverted.

An "active-site mobile loop", as referred to in the literature,[28] controls the entry of the substrate/inhibitor into the active site but has not been detected in the electron density maps of the X-ray structures. The "active-site mobile loop" was observed in our homology models as a discontinuous β-sheet structure (labeled B5 and B6) in the C-terminal domain (Figure 3a,b), after conjugate gradient minimization. The simulations of this loop show that it can adopt a wide range of low-energy conformations as seen in Figure 3a,b, which accounts for its flexibility and, hence, absence in the X-ray diffraction electron density maps. The developed models were checked for 3D compatibility using a 3D profile, the results of which are presented in the Supporting Information (file 2, Figure 1a,b). As observable from the figures, most of the residues are in a reasonable range. Only the variable regions R204−L206 in *E. coli* LpxC and R170−D177 in *P. aeruginosa* LpxC have been built poorly and could be considered as unreliable. Fortunately, these regions are located far from the active site and, thus, should not have much influence on the binding site interaction of ligands. Further, to assess the quality of the modeled structures, Ramachandran plots in the PROCHECK validation package were produced. For the refined *E. coli* LpxC model, 97.9% of the residues were in the allowed region, 1.6% in the generously allowed region, and only 0.4% in the disallowed region (Supporting Information, file 2, Figure 2a). In the case of the *P. aeruginosa* LpxC model, 99.2% of the residues were in the allowed region and 0.4% each in the generously allowed and disallowed regions (Supporting Information, file 2, Figure 2b). This indicates that the backbone dihedral angles Φ and ψ in the model were reasonably accurate. The

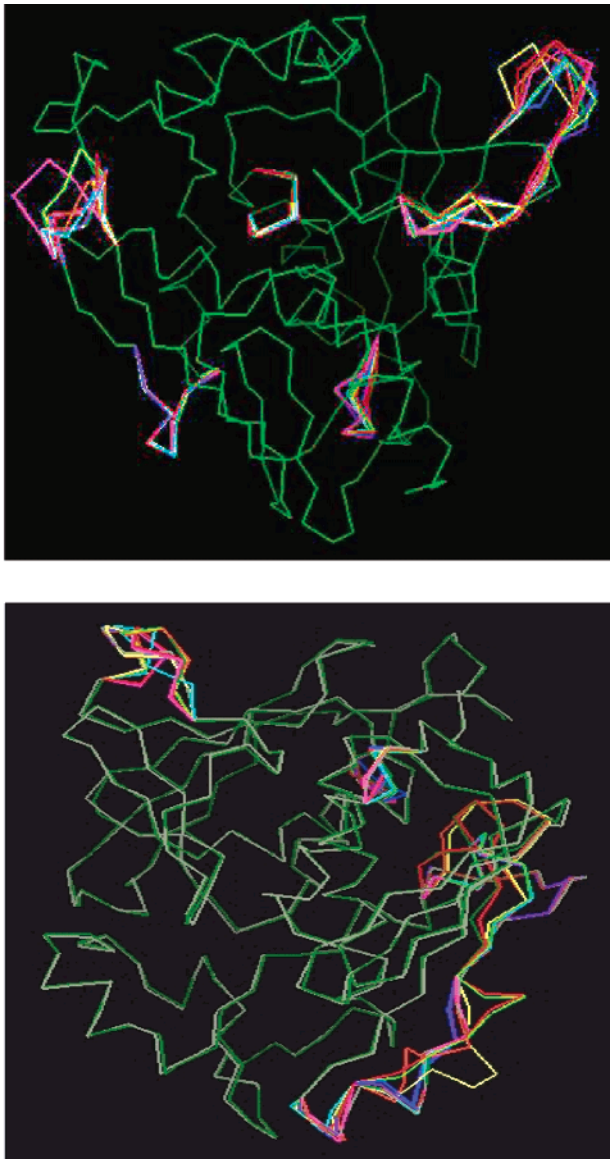

Figure 3. (a and b) A display of the 10 structures from the conjugated minimization of the active mobile loop in the *E. coli* LpxC and *P. aeruginosa* LpxC models.

two residues in the disallowed regions, for both models, were not a part of the active sites under investigation. The RMS deviation of the *E. coli* LpxC and *P. aeruginosa* LpxC final models with the template *A.aeolicus* deacetylase LpxC (1P42) at the C-α region was calculated to be 1.00 and 1.62 Å, respectively, and 0.93 and 1.58 Å, respectively, in the backbone region. This indicates that the model was sufficiently accurate for further structure-based analysis.

Topology of *E. coli* LpxC and *P. aeruginosa* LpxC. The overall fold of LpxC belongs to the α+β class, and the tertiary structure is formed by two major domains connected by a 16-residue linker. In *E. coli* LpxC, each domain consists of a five-stranded β sheet and two principal α helices; the two domains assemble so that the β sheets sandwich the α helices (Figure 4a). However, in *P. aeruginosa* LpxC, each domain consists of a four-stranded β sheet and two principal α helices. Here too, the two domains assemble so that the β sheets sandwich the α helices (Figure 4b). In both the models, each domain has an identical topology of secondary structural elements despite insignificant amino acid sequence identity.

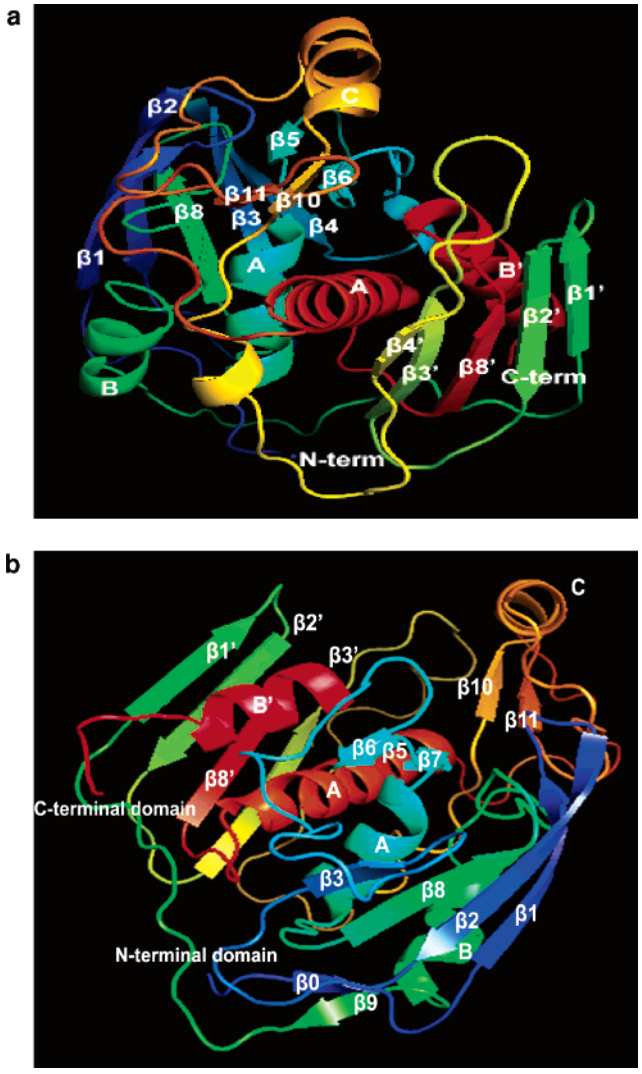

Figure 4. (a and b) Structural topology of *E. coli* LpxC and *P. aeruginosa* LpxC obtained by comparative modeling. α helices are colored red, and *β* strands (B) are colored green, cyan, yellow, and blue. N and C indicate the N-terminal and C-terminal regions of the protein. Hs and Bs are numbered along the amino acid sequence from the N- to C-terminal region.

The active site is located at the interface of the two domains and is also flanked by two smaller subdomains: a *βββ* subdomain inserted between *β* strand 4 and helix A and a *βαβ* subdomain inserted between *β* strand 4′ and helix A. It is noticeable that even though coordinates for the *β*4 strand were assigned from the *A. aeolicus* Lpxc deacetylase (1P42), where it appears as a strand, it occurred as a loop in the *P. aeruginosa* LpxC final structure, despite the good similarity in active-site region.

***E. coli* LpxC−*P. aeruginosa* LpxC Active-Site Analysis.** The active-site analysis performed using the siteID program in SYBYL7.1 revealed certain differences between the *E. coli* and *P. aeruginosa* LpxC active sites. For both proteins, according to functionality, the binding site has been referred to as deep, conical active-site cleft with a separate ∼15-Å-long hydrophobic tunnel at the bottom (Supporting Information, file 3, Figure 1a,b).[28] This hydrophobic tunnel is framed by the *βαβ* subdomain and is lined by several conserved aliphatic residues along with a solvent-accessible pocket. In *E. coli* LpxC, the active site is flat and narrow with the bottom hydrophobic tunnel being more lipophilic in nature

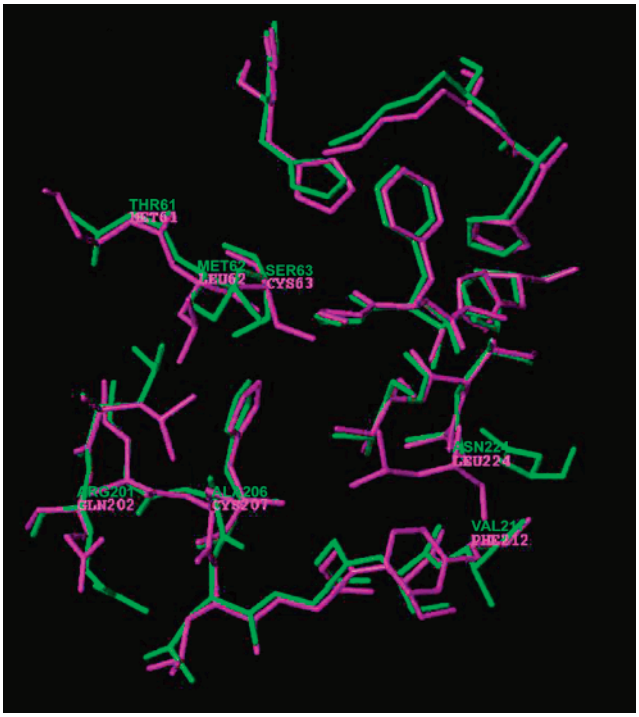

Figure 5. Active site residues of *E. coli* LpxC (magenta) superposition onto the *P. aeruginosa* LpxC (green), the difference in active site indicated by different amino acids labled.

(LP = 0.02−0.06) as compared to the hydrophobic tunnel in the active site of *P. aeruginosa* LpxC (LP = −0.035 to −0.029). These active site differences have been further studied using MEP and a cavity-depth analysis algorithm.

Biochemical studies by Jackman et al. on *A. aeolicus* LpxC showed that the substrate like 3-O-(*R*-3-hydroxymyristoyl) makes key interactions (required for optimal binding and catalysis) within the hydrophobic tunnel, by stabilizing the conformation of the *βαβ* subdomain that forms one wall of the active-site cleft. The catalytic Zn^{2+}A ion is more deeply situated in the active site than the inhibitory Zn^{2+}B ion and is coordinated by H79, H238, and D242 or D246 of helix A.[28,37] Notably, the direct zinc ligands are located on topologically equivalent helices at the domain−domain interface. Histidine ligations to the catalytic zinc ion have been identified in recent mutagenesis studies.[35,36] The HKX (L,F)D sequence motif is found in all currently available LpxC sequences (boldface, direct zinc ligands; X, aliphatic residues M, I, L, V, T, and A). This sequence represents an alternate zinc-recognition motif (Figure 2a,b; dark-gray-color box). Site-directed mutagenesis studies of LpxC from *E. coli* LpxC indicate that invariant residues H79 and H238 are important for catalysis; moreover, the decreased susceptibility of H79 variants to inhibition by zinc suggests that H79 coordinates to an inhibitory zinc ion.[39] A few other invariant or highly nonconserved residues are found in the active site of *E. coli* LpxC.

Characteristic differences in the active site were revealed by superpositioning the homology model of *E. coli* LpxC over *P. aeruginosa* LpxC (Figure 5). The residues Met61, Leu62, Cys63, Leu 224, Phe212, Cys207, and Gln202 in *E. coli* LpxC are replaced by Thr61, Met62, Ser63, Asn224, Val211, Ala206, and Arg201 in *P. aeruginosa* LpxC, respectively. These differences in the active-site residues should undoubtedly affect the steric and electrostatic interac-

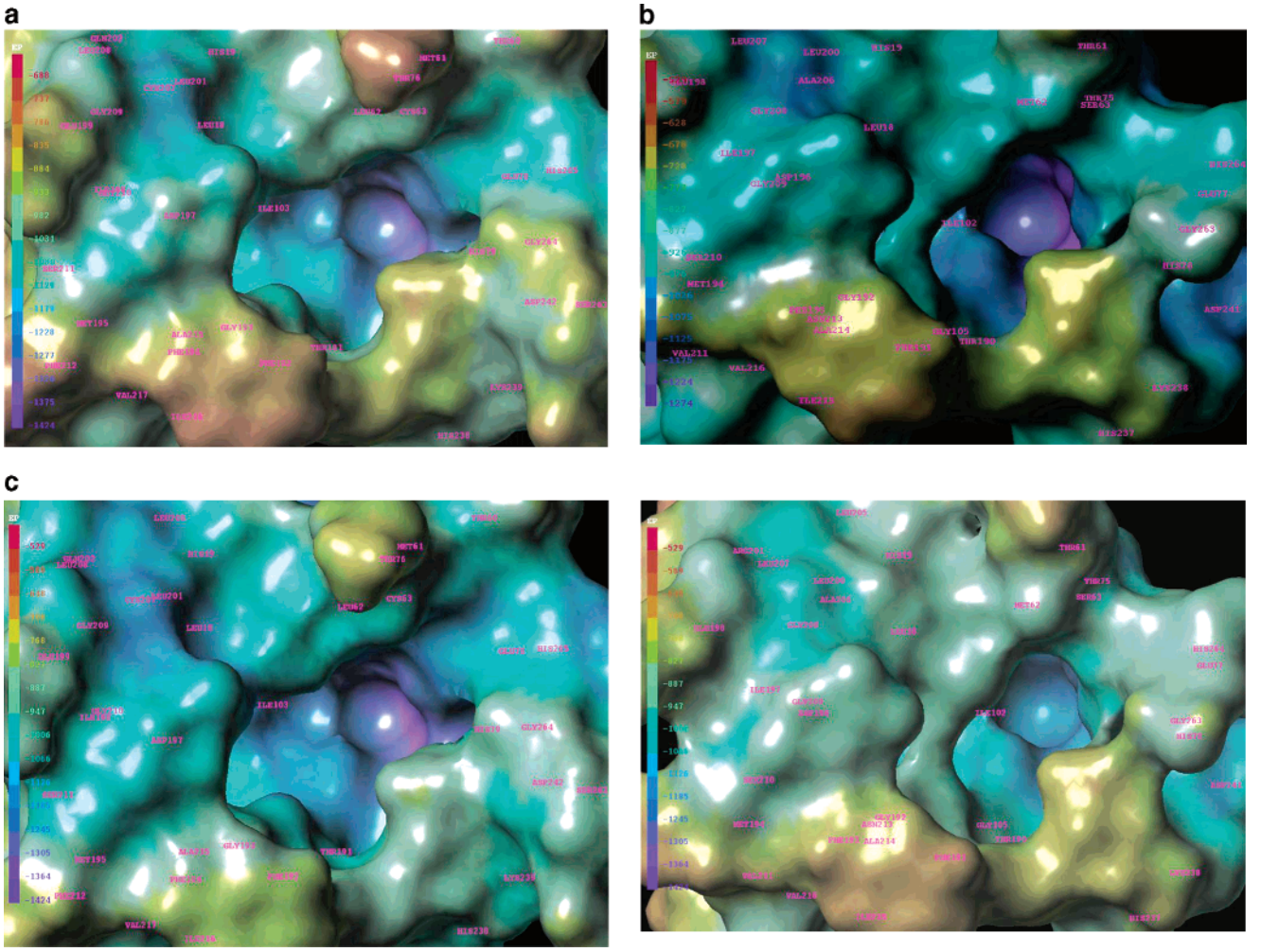

Figure 6. Absolute molecular electrostatic potential (MEP) values displayed for active sites of *E. coli* LpxC (a) and *P. aeruginosa* LpxC (b). The deep purple color indicates the highest negative potential, whereas the most positive potential is seen as a deep yellow-red color. The color spectrum shown to the left shows the gradation of electrostatic potential in the respective enzymes. In order to make valid comparisons between two models, the electrostatic potentials have been put on the same scale (c).

tions with inhibitors. MEP is a popular indicator of electrophilic and nucleophilic centers, which governs the strength of bonded and nonbonded interactions and molecular reactivity. It affects the strength of interactions of the ligand with a receptor protein. Bhattacharrjee and Karle have used MEP to relate the antimalarial potency of carbinolamine analogs[39] and the neurotoxicity of artemisinin analogs.[40] In the case of ligand−protein interactions, the ligand experiences a unique environment in terms of electrostatic, steric, and hydrophobic properties at the active site. Variations in these properties in the active sites of different proteins can contribute to selective/specific or tighter binding of the ligand to enzyme proteins. Thus, a comparison of the MEP of *E. coli* and *P. aeruginosa* LpxC's would be one step toward understanding the differential susceptibility of these two species to given inhibitors. The MEP surfaces depicted in Figure 6 are shown with absolute values of the electrostatic potential for *E. coli* LpxC (−688 to −1424 kcal/mol Å; Figure 6A) and *P. aeruginosa* LpxC (−527 to −1274 kcal/mol Å; Figure 6B). Since the range of potentials in the two proteins is varying, the two proteins were placed on the same scale of electrostatic potential (−529 to −1424 kcal/mol Å; Figures 6C) to make the comparison easier. As is evident in Figure 6C, the electrostatic potentials covering the active-site residues in the two proteins have sharply differing values. Within the *E. coli* LpxC active site, the surface around Ile103, Leu18, Leu201, Cys212, and Gly209 residues has a relatively more electronegative potential than that created by Ile102, Leu18, Leu200, Ala206, and Gly208 residues within the *P. aeruginosa* LpxC active site. Moreover, a contrasting feature is also visible for the region encompassing residues Thr191, His238, Lys239, His79, and Gly264 within the *E. coli* LpxC active site which is less electropositive as compared to the corresponding residues, Thr190, His237, Lys238, His78, and Gly263, within the *P. aeruginosa* LpxC active site. Further, the difference in the value of the potential at His79 and His238 in *E. coli* LpxC (−887 to −947 kcal/mol Å) and His78 and His237 in *P. aeruginosa* LpxC (−768 to −827 kcal/mol Å) might have a good impact on the variable binding to Zn^{2+} which is responsible for the catalytic activity in LpxC. This implies that the two proteins could bind the inhibitors in the same relative sense, but with different binding affinities, due to the differences in the absolute values of the electrostatic potential.

Subsequently, a cavity-depth analysis of both proteins revealed differences in the active-site cleft near the Zn^{2+} binding pocket (Supporting Information, file 4, Figure 1). In the case of *E. coli* LpxC, the area at the bottom of the active-site cleft has a depth value of 4.4−5.2 Å, which is different from the corresponding area in the *P. aeruginosa*

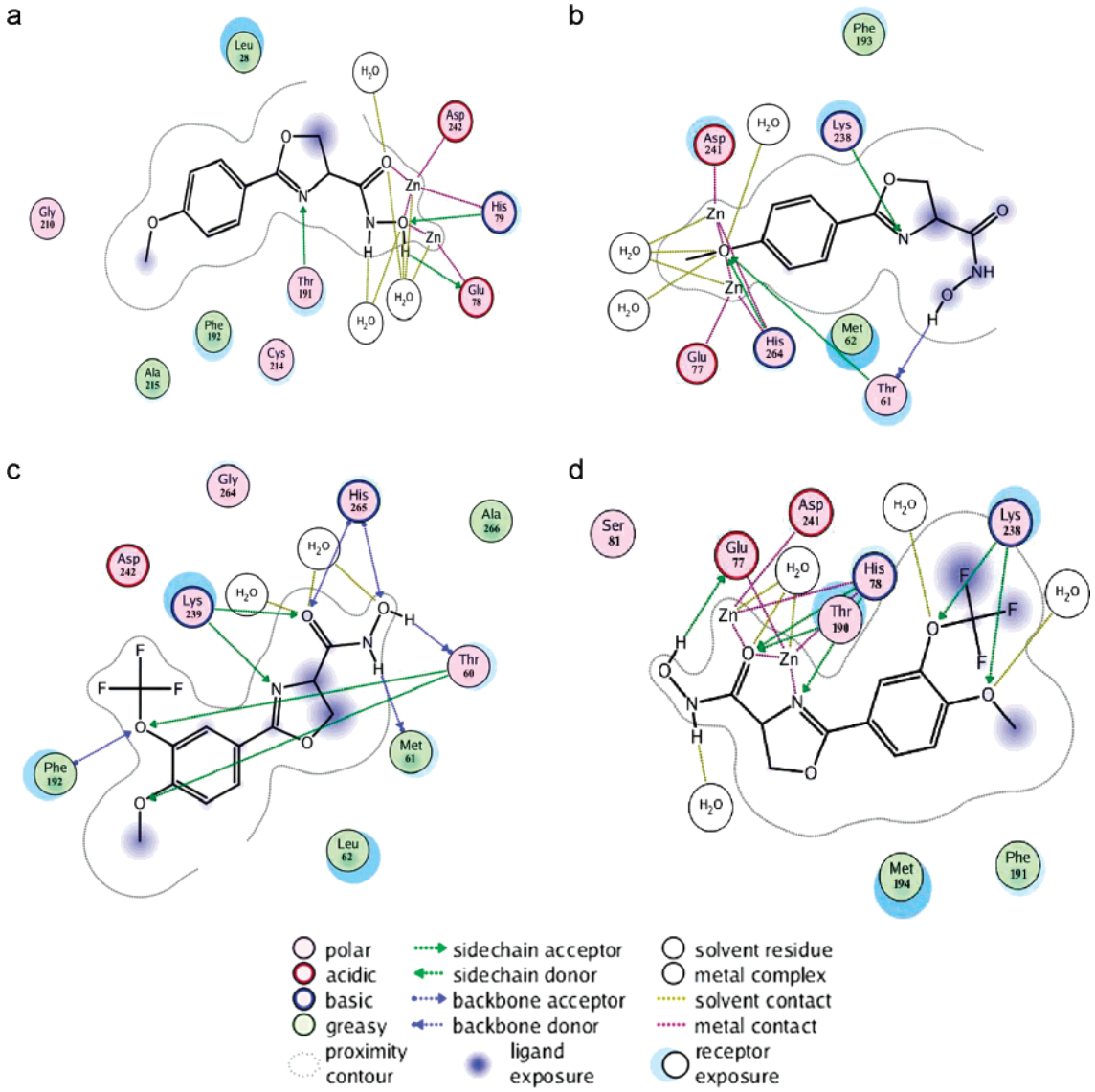

Figure 7. Selectively docked molecules in homology models of the *E. coli* and *P. aeruginosa* LpxC active site. Parts a and b indicate the docking of **1B1** into the *E. coli* and *P. aeruginosa* LpxC. Parts c and d indicate the docking of the **1B2** into the *E. coli* and *P. aeruginosa* LpxC.

LpxC active site, which has a depth value of 4.7−6.3 Å. These differences in active sites of the two proteins can possibly make a reasonable contribution toward selective binding of the inhibitors (Figure 6). Thus, along with MEP, a cavity-depth analysis provided basic differences of active sites of the two proteins. However, it was speculated that molecular docking of the known inhibitors of *E. coli* LpxC and *P. aeruginosa* LpxC on the active site of both proteins could provide a clearer and more-accurate understanding of active-site residue interaction and the selective binding mode of inhibitors.

Thus, to study the active-site interaction of known potent inhibitors against these targets, a molecular docking study on the developed homology models was performed. One of the templates used for homology modeling (*A. aeolicus* LpxC) is a cocrystal with the TU-514 ligand (PDB ID: 1XXE). Thus, to validate the docking protocol, TU-514 was extracted from the crystal structure of LpxC and docked into the *E. coli* LpxC and *P. aeruginosa* LpxC homology models. A set of 30 conformations during the docking of each ligand was generated (Supporting Information, file 5, Figure 1A−D; Table 1A−D), from which the one with the highest consensus score was selected. The docked TU-514 showed essentially the same conformation as the bound ligand with RMS values of 0.702 and 0.892 Å in *E.coli* and *P. aeruginosa* LpxC models, respectively, calculated using the FIT ATOM method in SYBYL 7.1.

Once the docking methodology was validated, the same protocol was used for the reported potent inhibitors of *E. coli* LpxC (i.e., **1B1**) and *P. aeruginosa* LpxC (i.e., **1B2**). Most of the amino acids, that is, Val174, Leu253, Gly85, Phe152, Ala84, Val182, Leu240, Val111, Val185, Leu243, Phe181, and Ser252, are common to the binding pockets of both LpxC proteins. The cross-docking approach, that is, docking the same molecule in both homology models to study the comparative binding mode of these inhibitors, was used.

Whereas, in the *P. aeruginosa* LpxC active site, the hydroxamic moiety of **1B1** did not make any interactions with Zn^{2+} (Figure 7b), which is actually necessary for inhibition. Biological studies reported **1B1** to be more selective for *E. coli* LpxC as compared to *P. aeruginosa*

Table 2. Docking Scores and Interactions of **1B2** and **1B1** with Developed Homology Model of *E. coli* and *P. aeruginosa* LpxC

					Interactions		
protein	compounds	score	H-bond	residues involved	π-stacking	H-phobic	residues involved
P. aeruginosa LpxC	1B2	−19.98	3	Asp241, His264, Glu77	Phe 181	6	Val174, Leu253, Gly 85, Phe 152, Ala 84, Phe 181
	1B1	−19.32	3	Asp242, His79, Glu78		6	Phe181,Val174, Leu253, Phe 152, Val 182, Val185
E. coli LpxC	1B2	−22.02	4	Thr198, Asp242, His79, Glu78		7	Leu201,Gly 193, Ala 215, Thr191, His 79, ys 239, Cys63
	1B1	−23.54	3	Met61, Thr68, His265		8	Thr191,His 79, Lys 239, Cys63, Leu201, Gly 210,Gly193, Ile103

LpxC. According to our analysis, a possible cause for this could be the difference of 1−1.2 Å in the cavity depth of active sites of the two proteins along with a reduced hydrophobicity at the bottom of the cavity. The *P. aeruginosa* binding site buries the phenyl ring of the ligand in its cavity while leaving the hydroxamic acid floating in the hydrophobic pocket. The phenyl ring possibly interacts with Asp241, Glu77, and His78. The hydrophobic interactions seem to contribute significantly to the overall binding (Table 2). A corresponding difference has been observed in the docking score of **1B1** in both active sites. The main reason predicted from the above observation is the hydrophobic nature of the active site which contributes more toward the selective binding of **1B1** into the *E. coli* LpxC and *P. aeruginosa* LpxC active sites, along with cavity-depth differences.

Subsequently, we performed docking of **1B2** in both models (Figure 7c,d). The docked **1B2** essentially adopted a butterflylike conformation within the *P. aeruginosa* LpxC binding pocket (Figures 7d). Moreover, in accordance with the reported experimental studies for LpxC substrate/inhibitors,[37] the docked ligands could adopt a collection of alternative positions that were anchored by the hydroxamic acid group but left the phenyl ring free to pivot inside the hydrophobic pocket. The hydroxyl oxygen and nitrogen of hydroxamic acid made hydrogen-bonding interactions with Glu77, Asp241, His78, and Thr198 via Zn^{2+} (Figure 7d). The side-chain donor Lys238 interacted with the oxygen of trifluoromethoxy and the hydroxyl group of the phenyl ring while the phenyl moiety π-stacked against the Phe181.

A similar binding mode was not observed for **1B2** when docked into the *E.coli* LpxC model (Figure 7c). Here, the phenyl ring adopted a slightly flat conformation as compared to the previous butterflylike orientation. Because the active site in E .*coli* LpxC is flat, narrow, and shallow, the hydroxamic acid group of **1B2** was unable to reach inside the site where it could possibly interact with an amino acid residue via the Zn^{2+} ion. In this case, His265 and Lys239 act as backbone and side-chain donors, respectively, and Met61 and Thr60 as backbone acceptors. π-Stacking interactions were not observed in this case. Thus, the selectivity of binding of these known LpxC inhibitors toward *E. coli* and *P. aeruginosa* LpxC's can mainly be attributed to the hydrophobic nature of the active site along with cavity-depth differences. In the case of *E. coli* LpxC, the hydrophobic nature of the active site is due to the presence of Thr191, His79, Lys239, Cys63, Leu201, Gly 210, Gly193, and Ile103 residues (Supporting Information, file 3, Figure 1a). Whereas, in the case the active site of *P. aeruginosa* LpxC, it consists of Phe181, Val174, Leu253, Phe152, Val 182, and Val185 hydrophobic residues (Supporting Information, file 3, Figure 1b).

CONCLUSIONS

The present study concludes an in silico structural and cavity-depth analysis of LpxC from *E. coli* and *P. aeruginosa* species and provides a structural rationale for the differential susceptibilities of these species to known *E. coli* LpxC inhibitors. A 3D model of LpxC for *E. coli* LpxC and *P. aeruginosa* LpxC was constructed by a homology modeling technique. This resulted in reliable modeling of the ligand-binding domain and shed new light on the binding features of this enzyme, which has not yet been crystallized. In particular, significant differences in the active sites for *E. coli* and *P. aeruginosa* LpxC's were identified. The model suggested several minor but potentially important structural differences in the catalytic binding domain of the two proteins. Structural differences identified in this study might facilitate the design of inhibitors with broad-spectrum LpxC inhibitory activity. Thus, the in silico study suggests that strategies to identify broad-spectrum LpxC inhibitors could be challenging unless the structural differences in LpxC enzymes from different Gram-negative bacterial species are considered.

Supporting Information Available: Crystal structure template; distances measured between atom pairs in comparison to template 1P42; 3D-profile window plots for homology models *E. coli* LpxC and *P. aeruginosa* LpxC; PROCHECK Ramchandran plot for the homology model of *E. coli* LpxC and *P. aeruginosa* LpxC; active site analysis in the homology model of *E. coli* LpxC; active site analysis of homology model of *P. aeruginosa* deacetylase LpxC; absolute cavity depth analysis values displayed for active sites of *E. coli* LpxC and *P. aeruginosa* LpxC; binding site cluster after docking of 1B1 into EcLpxC and PaLpxC, and 1B2, docking into the EcLpxC and PaLpxC; and conformations of molecule, total score, RMS value of binding site cluster after docking of 1B1 into EcLpxC and PaLpxC, and 1B2, docking into the EcLpxC and PaLpxC. This material is available free of charge via the Internet at http://pubs.acs.org.

REFERENCES AND NOTES

(1) Vaara, M. Agents that Increase the Permeability of the Outer Membrane. *Microbiol. Mol. Biol. Rev.* **1992**, *56*, 395−411.
(2) Vuorio, R.; Vaara, M. The Lipid A Biosynthesis Mutation lpxA2 of *Escherichia coli* Results in Drastic Antibiotic Supersusceptibility. *Antimicrob. Agents Chemother.* **1992**, *36*, 826−829.
(3) Vaara, M. Outermembrane Permeability Barrier to Azithromycin, Clarithromycin and Roxithromycin in Gram-Negative Enteric Bacteria. *Antimicrob. Agents Chemother.* **1993**, *37*, 354−356.
(4) Nikaido, H.; Vaara, M. Molecular Basis of Bacterial Outer Membrane Permeability. *Microbiol. Rev.* **1985**, *49*, 1−32.
(5) Raetz, C. R. H. Biochemistry of Endotoxins. *Annu. Rev. Biochem.* **1990**, *59*, 129−170.

(6) Raetz, C. R. H. Bacterial Endotoxins: Extraordinary Lipids that Activate Eukaryotic Signal Transduction. *J. Bacteriol.* **1993**, *175*, 5745−5753.
(7) Onishi, H. R.; Pelak, B. A.; Gerckens, L. S.; Silver, L. L.; Kahan, F. M.; Chen, M. H.; Patchett, A. A.; Galloway, S. M.; Hyland, S. A.; Anderson, M. S.; Raetz, C. R. H. Antibacterial Agents that Inhibit Lipid A Biosynthesis. *Science* **1996**, *274*, 980−982.
(8) Wyckoff, T. J.; Raetz, C. R. H.; Jackman, J. E. Antibacterial and Anti-Inflammatory Agents that Target Endotoxin. *Trends Microbiol.* **1998**, *6*, 154−159.
(9) Vaara, M. Lipopolysaccharide and the Permeability of the Bacterial Outer Membrane. In *Endotoxin in Health and Disease*, 1st ed.; Brade, H., Opal, S. M., Vogel, S. N., Morrison, D. C., Eds.; Marcel Dekker: New York, 1999; pp 31−32.
(10) Rick, P. D.; Raetz, C. R. H. Microbial Pathways of Lipid A Biosynthesis. In *Endotoxin in Health and Disease*, 1st ed.; Brade, H., Opal, S. M., Vogel, S. N., Morrison, D. C., Eds.; Marcel Dekker: New York, 1999; pp 283−304.
(11) Anderson, M. S.; Bulawa, C. E.; Raetz, C. R. The Biosynthesis of Gram-Negative Endotoxin Formation of Lipid A Precursors from UDP-GlcNAc in Extracts of *Escherichia coli*. *J. Biol. Chem.* **1985**, *260*, 15536−15541.
(12) Anderson, M. S.; Robertson, A. D.; Macher, I.; Raetz, C. R. H. Biosynthesis of Lipid A in *Escherichia coli*: Identification of UDP-3-*O*-[*R*-3-hydroxymyristoyl]-R-D-glucosamine. *Biochemistry* **1988**, *27*, 1908−1917.
(13) Anderson, M. S.; Bull, H. G.; Galloway, S. M.; Kelly, T. M.; Mohan, S.; Radika, K.; Raetz, C. R. H. UDP-*N*-acetylglucosamine Acyltransferase of *Escherichia coli*. The First Step of Endotoxin Biosynthesis Is Thermodynamically Unfavorable. *J. Biol. Chem.* **1993**, *268*, 19858−19865.
(14) Young, K.; Silver, L. L.; Bramhill, D.; Cameron, P.; Eveland, S. S.; Raetz, C. R. H.; Hyland, S. A.; Anderson, M. S. The envA Permeability/Cell Division Gene of *Escherichia coli* Encodes the Second Enzyme of Lipid A Biosynthesis. UDP-3-*O*-(*R*-3-hydroxymyristoyl)-*N*-acetylglucosamine Deacetylase. *J. Biol. Chem.* **1995**, *270*, 30384−30391.
(15) Beall, B.; Lutkenhaus, J. Sequence Analysis, Transcriptional Organization, and Insertional Mutagenesis of the envA Gene of *Escherichia coli*. *J. Bacteriol.* **1987**, *169*, 5408−5415.
(16) Jackman, J. E.; Fierke, C. A.; Tumey, L. N.; Pirrung, M.; Uchiyama, T.; Tahir, S. H.; Hindsgaul, O.; Raetz C. R. H. Antibacterial Agents that Target Lipid A Biosynthesis in Gram-Negative Bacteria. Inhibition of Diverse UDP-3-O-(R-3-hydroxymyristoyl)-N-acetylglucosamine Deacetylases by Substrate Analogs Containing Zinc Binding Motifs. *J. Biol. Chem.* **2000**, *275*, 11002−11009.
(17) Jacobs, M. A.; Alwood, A.; Thaipisuttikul, I.; Spencer, D.; Haugen, E.; Ernst, S.; Will, O.; Kaul, R.; Raymond, C.; Levy, R.; Chun-Rong, L.; Guenthner, D.; Bovee, D.; Olson, M. V.; Manoil, C. Comprehensive Transposon Mutant Library of *Pseudomonas aeruginosa*. *Proc. Natl. Acad. Sci. U.S.A.* **2003**, *100*, 14339−14344.
(18) Hyland, S. A.; Eveland, S. S.; Anderson, M. S. Cloning, Expression, and Purification of UDP-3-O-acyl-GlcNAc Deacetylase from *Pseudomonas aeruginosa*: A Metalloamidase of the Lipid A Biosynthesis Pathway. *J. Bacteriol*. **1997**, *179*, 2029−2037.
(19) Clements, J. M.; Coignard, F.; Johnson, I.; Chandler, S.; Palan, S.; Waller, A.; Wijkmans, J.; Hunter, M. G. Antibacterial Activities and Characterization of Novel Inhibitors of LpxC. *Antimicrob. Agents Chemother*. **2002**, *46*, 1793−1799.
(20) Pirrung, M. C.; Tumey, L. N.; McClerren, A. L.; Raetz, C. R. H. High-Throughput Catch and Release Synthesis of Oxazoline Hydroxamates. Structure−Activity Relationships in Novel Inhibitors of *Escherichia coli* LpxC: *In-vitro* Enzyme Inhibition and Antibacterial Properties. *J. Am. Chem. Soc*. **2003**, *125*, 1575−1586.
(21) Pirrung, M. C.; Tumey, L. N.; Raetz, C. R. H.; Jackman, J. E.; Snehalatha, K.; McClerren, A. L.; Fierke, C. A.; Gantt, S. L.; Rusche, K. M. Inhibition of the Antibacterial Target UDP-(3-O- acyl)-N-acetylglucosamine Deacetylase (LpxC): Isoxazoline Zinc Amidase Inhibitors Bearing Diverse Metal Binding Groups. *J. Med. Chem.* **2002**, *45*, 4359−4370.
(22) Mdluli, K. E.; Witte, P. R.; Kline, T.; Barb, A. W.; Erwin, A. L.; Mansfield, B. E.; McClerren, L.; Pirrung, M. C.; Tumey, L. N.; Warrener, P.; Raetz, C. R. H.; Stover, C. K. Molecular validation of LpxC as an antibacterial drug target in *Pseudomonas aeruginosa*. *Antimicrob. Agents Chemother*. **2006**, *50*, 2178−2184.
(23) Kline, T.; Andersen, N. H.; Harwood, E. A.; Bowman, J.; Malanda, A.; Endsley, S.; Erwin, A. L.; Doyle, M.; Fong, S.; Harris, A. L.; Mendelsohn, B.; Mdluli, K.; Raetz, C. R. H.; Stover, C. K.; Witte, P. R.; Yabannavar, A.; Zhu, S. Potent, Novel *In-Vitro* Inhibitors of the *Pseudomonas aeruginosa* Deacetylase LpxC. *J. Med. Chem*. **2002**, *45*, 3112−3129.
(24) *MOE*, version 06; Chemical Computing Groups Inc.: Montreal, Canada.
(25) *SYBYL*, version 7.1; Tripos Associates Inc.: St. Louis, MO.
(26) Altschul, S. F.; Gish, W.; Miller, W.; Myers, E. W.; Lipman, D. J. Basic Local Alignment Search Tool. *J. Mol. Biol*. **1990**, *215*, 403−410.
(27) Berman, H. M.; Westbrook, J.; Feng, Z.; Gilliland, G.; Bhat, T. N.; Weissig, H.; Shindyalov, I. N.; Bourne, P. E. The Protein Data Bank. *Nucleic Acids Res.* **2000**, *28*, 235−242.
(28) Whittington, D. A.; Rusche, K. M.; Shin, H.; Fierke, C. A.; Christianson, D. W. Crystal Structure of LpxC, a Zinc-Dependent Deacetylase Essential for Endotoxin Biosynthesis. *Proc. Natl. Acad. Sci. U.S.A.* **2003**, *100*, 8146−8150.
(29) Coggins, B. E.; McClerren, A. L.; Jiang, L.; Li, X.; Rudolph, J.; Hindsgaul, O.; Raetz, C. R. H.; Zhou, P. Refined Solution Structure of the LpxC-TU-514 Complex and pk(a) Analysis of an Active Site Histidine: Insights into the Mechanism and Inhibitor Design. *Biochemistry* **2005**, *44*, 1114−1126.
(30) Hickman, A. B.; Li, Y.; Mathew, S. V.; May, E. W.; Craig, N. L.; Dyda, F. Unexpected Structural Diversity in DNA Recombination: The Restriction Endonuclease Connection. *Mol. Cell*. **2000**, *5*, 1025−1034.
(31) Luthy, R.; Bowie, J. U.; Eisenberg D. Assessment of Protein Models with Three-Dimensional Profiles. *Nature* **1992**, *356*, 83−85.
(32) Laskowski, R.; MacArthur, M.; Moss, D.; Thornton, J. PROCHECK: A Program to Check the Stereochemical Quality of Protein Structures. *J. Appl. Crystallogr*. **1993**, *26*, 283−291.
(33) Dewar, J. S.; Zoebisch, E. G.; Healy E. F. AM1: A New General Purpose Quantum Mechanical Molecular Model. *J. Am. Chem. Soc.* **1985**, *107*, 3902−3909.
(34) Mulliken, R. S. Electronic Population Analysis on LCAO-MO Molecular Wave Function I. *J. Chem. Phys.* **1955**, *23*, 1833−1846.
(35) McClure, C. P.; Rusche, K. M.; Peariso, K.; Jackman, J.; Fierke, C. A.; Penner-Hahn, J. E. EXAFS Studies of the Zinc Sites of UDP-(3-O-acyl)-N-acetylglucosamine Deacetylase (LpxC). *J. Inorg. Biochem.* **2003**, *94*, 78−85.
(36) Jackman, J. E.; Raetz, C. R.; Fierke, C. A. Site-Directed Mutagenesis of the Bacterial Metalloamidase UDP-(3-O-acyl)-N-acetylglucosamine Deacetylase (LpxC). Identification of the Zinc Binding Site. *Biochemistry* **2001**, *2*, 514−523.
(37) Hernick, M.; Gennadios, H. A.; Whittington, D. A.; Rusche, K. M.; Christianson, D. W.; Fierke, C. A. UDP-(3-O-(*R*-3-hydroxymyristoyl))-N-acetylglucosamine Deacetylase Functions through a General Acid−Base Catalyst Pair Mechanism. *J. Biol. Chem.* **2005**, *280*, 16969−16978.
(38) Needleman, S. B.; Wunsch, C. D. A General Method Applicable to the Search for Similarities in the Amino Acid Sequence of Two Proteins. *J. Mol. Biol*. **1970**, *48*, 443−453.
(39) Bhattacharjee, A. K.; Karle, J. M. Functional Correlation of Molecular Electronic Properties with Potency of Synthetic Carbinolamines Antimalarial Agents. *Bioorg. Med. Chem*. **1998**, *6*, 1927−1933.
(40) Bhattacharjee, A. K.; Karle, J. M. Stereoelectronic Properties of Antimalarial Artemisinin Analogues in Relation to Neurotoxicity. *Chem. Res. Toxicol*. **1999**, *12*, 422−428.

CI6004806